RAA 2019 Vol. **19** No. **7**, 96(8pp) doi: 10.1088/1674–4527/19/7/96

http://www.raa-journal.org *http://iopscience.iop.org/raa*

***R**esearch in*
***A**stronomy and*
***A**strophysics*

Radio spectral index from NVSS and TGSS

Prabhakar Tiwari

National Astronomical Observatories, Chinese Academy of Sciences, Beijing 100101, China; *ptiwari@nao.cas.cn*

Received 2018 November 2; accepted 2019 January 29

Abstract I extract the radio spectral index, α, from 541 195 common sources observed in the 150 MHz TIFR GMRT Sky Survey (TGSS) and the 1.4 GHz NRAO VLA Sky Survey (NVSS). This large common source catalog covers about 80% of the sky. The flux density limits in these surveys are such that the observed galaxies are presumably hosts of active galactic nuclei (AGNs). I confirm the steepening of α with increasing flux density for this large sample and provide a parametric fit between α and flux density. Next, I divide the data into low flux (LF) and high flux (HF) density samples with roughly equal numbers of galaxies. The LF sample contains all galaxies below 100 mJy TGSS and 20 mJy NVSS flux density and the HF sample is all galaxies above 100 mJy TGSS and 20 mJy NVSS. I observe an increase in α with source size (TGSS measured), saturating for large sizes to 0.89 ± 0.22 and 0.76 ± 0.21 for the LF and HF sources, respectively. I discuss the observed results and possible physical mechanisms to explain observed α dependence with source size for LF and HF samples.

Key words: galaxies: high-redshift — galaxies: active galactic nuclei

1 INTRODUCTION

The radio emission from a distant galaxy consists of thermal and synchrotron contributions. The thermal emission is bremsstrahlung radiation from HII regions while the non-thermal synchrotron emission is generated by supernova remnants (SNRs), diffuse cosmic ray electrons (CREs) spread over the disk and halo (Biermann 1976; Condon 1992), and relativistic plasma in jets and jet fed lobes (De Young 1976; Blandford & Königl 1979). The bright radio galaxies, relevant to flux density limits in this work, are hosts of active galactic nuclei (AGNs) and their radio emission is predominantly synchrotron radiation from jets of relativistic plasma and jet fed lobes[1]. These emission components are characterized by different spectral indices and, therefore, the total spectral index depends on their relative contributions. The thermal emission is almost flat ($\propto \nu^{-\alpha}$) with spectral index $\alpha_{\rm th} \approx 0.1$ (Condon 1992), whereas, the radio jets exhibit a spectral index $\alpha_{\rm jet} = 0.5 - 0.7$ (Bridle & Perley 1984; Laing & Bridle 2013) and the radio emission from lobes can be flat to very steep depending on energy injection and losses (Kellermann 1966).

I compile a common source catalog from the TIFR GMRT Sky Survey's First Alternative Data Release (TGSS ADR1) (Intema et al. 2017) and NRAO VLA Sky Survey (NVSS) (Condon et al. 1998) catalog, and use it to explore radio spectral index, size and flux density dependence. I identify a total of 541 195 sources which are common to both TGSS ADR1 and NVSS. The large sample allows spectral index values to be separated into differential source size bins and I obtain statistically significant dependence of spectral index on flux density and size. Assuming that the NVSS source population peaks between redshift $z \approx 0.5 - 1$ (Wilman et al. 2008; Nusser & Tiwari 2015; Tiwari & Nusser 2016), all results in this work statistically represent the radio source population at redshift $z \approx 0.8$.

The outline of the paper is as follows. I discuss the NVSS and TGSS ADR1 data and describe the cross-matching procedure in Section 2. In Section 3 I address the basic mechanisms of radio emission and their spectral index. I describe the observed spectral index in Section 4. In Section 5 I present all results. I conclude with discussion in Section 6.

[1] and the inverse-Compton scattering of the radio synchrotron emission within the lobes.

2 DATA

2.1 TGSS ADR1

The TGSS ADR1 catalog is based on the Giant Metrewave Radio Telescope (GMRT), performing an all-sky radio continuum survey at 150 MHz (Swarup 1991). The catalog was compiled between 2010 and 2012 and has been published recently by Intema et al. (2017). The catalog covers 90% of the full sky at 150 MHz with median root mean square (RMS) brightness fluctuations of 3.5 mJy beam^{-1} with approximate resolution $25'' \times 25''$ north of 19° Dec and $25'' \times 25''$/cos(Dec–19°) south of 19°. The best resolution observed with GMRT at 150 MHz is $20''$ (Lal 2013) and between declination $-20°$ and $+60°$. TGSS ADR1 sources are best resolved with resolution close to $20''$ (see figure 6 in Intema et al. (2017)). The catalog contains a total of 623 604 sources (489 570 sources above flux density [2] 50 mJy) observed at 6σ peak-to-noise threshold. The accuracy of the source centroid position is better than $2''$ (RMS). The catalog is almost complete above 100 mJy (Intema et al. 2017) and $\sim$ 70% complete above 50 mJy at 150 MHz.

2.2 NVSS

The NVSS catalog contains ∼1.8 million sources with flux densities $\mathrm{S}_{1.4\mathrm{GHz}} > 2.5$ mJy at 1.4 GHz (Condon et al. 1998). The full width at half maximum angular resolution is $45''$ and nearly all observations are performed at uniform sensitivity. The catalog covers about 82% of the sky and has a 100% overlap with TGSS ADR1. The RMS uncertainty in angular position is up to $7''$, substantially larger than TGSS. The catalog is complete above 3.5 mJy at 1.4 GHz.

2.3 TGSS-NVSS Common Source Catalog

Given the TGSS angular position for each of the 623 604 TGSS ADR1 sources, I identify NVSS sources within an angular distance less than $30''$. In total I find 553 301 TGSS ADR1 sources having at least one NVSS source within $30''$. Given the positional uncertainties of NVSS (Sect. 2.2) and TGSS ADR1 (Sect. 2.1), and with a criterion of $30''$, we have less than a 4σ chance of missing a source. Therefore due to positional uncertainty, we expect only to miss a few tens of sources while identifying NVSS matches for 0.6 million TGSS ADR1 sources. Furthermore, given the NVSS source number density, described in Section 2.2, there is a finite probability, ≈ 0.013, of having an NVSS source within a $30''$ radius and we expect to misidentify around 8000 sources due to this probability. Due to all these and other possible observational systematics and uncertainties (Condon et al. 1998; Intema et al. 2017) I find 12 106 sources, out of 553 301 cross-matched cases. These are either showing more than one NVSS association with search criteria of $30''$ or more than one TGSS source manifesting association with the same NVSS object. I drop these 12 106 sources to avoid confusion and artificial scatter in the spectral index. I end up with a total of 541 195 sources, identified in both TGSS ADR1 and NVSS. The common source counts for different TGSS flux density cuts are listed in Table 1. The spatial distribution of these common sources is shown in Figure 1.

Table 1 TGSS-NVSS Common Sources with Different TGSS Flux Density Cuts

$\mathrm{S}_{\mathrm{TGSS}}$ (mJy)	Number of sources
no cut	541 195
> 50	424 639
> 100	266 885
> 150	190 830
> 200	147 171

3 RADIO EMISSIONS IN AGNS

3.1 Thermal Radio Emission from HII Regions

The flux density of radio thermal emission dependence on frequency is expressed as (Condon 1992)

$$S_T \propto \nu^{-0.1} \,. \tag{1}$$

At high frequencies ($\sim$ GHz) where the electron deflection opacity is small, the ratio of non-thermal emission that approximates thermal radio emission S_T with respect to non-thermal radio emission S_{NT} is (Condon & Yin 1990)

$$S_{\mathrm{NT}} \sim 10 \left(\frac{\nu}{\mathrm{GHz}}\right)^{0.1-\alpha} S_T, \tag{2}$$

where $\alpha \sim 0.8$ is the approximate non-thermal spectral index (Intema et al. 2011; Williams et al. 2013, 2016; Hardcastle et al. 2016; Mahony et al. 2016b). This implies that the non-thermal emission is dominant with a thermal contribution of $\lesssim 10\%$ at 1.4 GHz and $\lesssim 3\%$ at 150 MHz.

3.2 Non-thermal Radio Emission

Radio galaxies are broadly categorized in Fanaroff & Riley (1974) type I (FR I) and type II (FR II) cases, and the large-scale structure of a radio galaxy roughly consists of three

[2] "flux density" refers to total flux density throughout the paper.

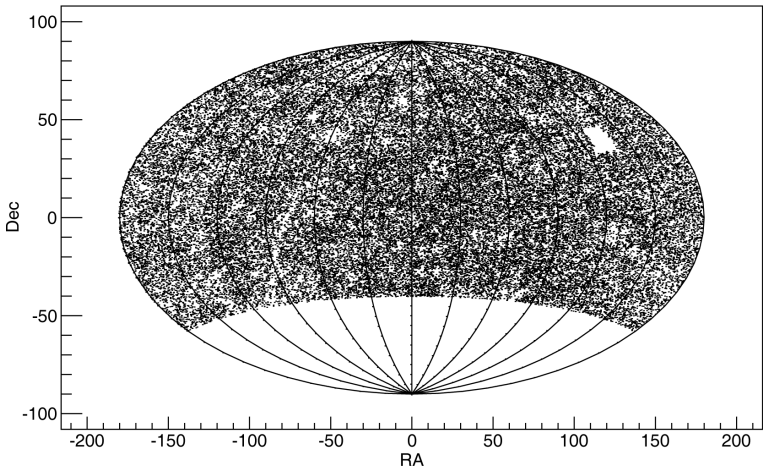

Fig. 1 The angular distribution of NVSS-TGSS common sources. Only 10% of randomly selected sources are plotted.

components: jets, lobes and hotspots (Harwood et al. 2013, 2015). In FR I galaxies, the jets are relatively less collimated and produce radio emission through deceleration (Laing & Bridle 2013, 2014), whereas the FR II jets are often non-emitting and the radio emission is largely produced in lobes and hotspots (Harwood et al. 2013, 2015).

3.2.1 Radio emission from jets

The relativistic jet transports material from the central AGN to extremities of the source and terminates as shock forming a hotspot, i.e. a compact region of synchrotron emission. At the point of acceleration, the electron number distribution is expressed as $N(E) \propto E^{-\gamma}$, where $\gamma \approx 2$ for FR I (Blandford & Königl 1979) and $\gamma > 2$ for FR II (Harwood et al. 2016, 2017). In FR I galaxies, for which the emission from jets is significant, the mean spectral index of radio emission from jets decreases with distance from the nucleus and $\alpha_{\rm jet} \approx 0.5 - 0.7$ (Laing & Bridle 2013).

3.2.2 Radio emission from jet fed lobes

The radio emission from extended radio-loud galaxies is dominated by radio lobes which are fed by collimated narrow jets. The radio emission from these lobes depends on electron injection and energy losses. For a continuous supply of electrons, the number distribution obtained by considering losses to synchrotron is $N(E) \propto E^{-1-\gamma}$ (Kellermann 1966), corresponding to $\alpha = \gamma/2$. If the energy injection is intermittent, then α depends on the frequency ν and the time interval between bursts. In this case, the first-order Fermi acceleration assuming strong shocks (Bell 1978; Blandford & Ostriker 1978; Kirk et al. 2000; Lemoine & Pelletier 2003) gives a relatively flat spectrum ($\alpha_{\rm lobes} \geq 0.5$) at low frequencies and a very steep one ($\alpha_{\rm lobes} = 1.33$) at higher frequencies (Kellermann 1966).

3.2.3 Radio emission from core

The spectral characteristics of "compact" (i.e., unresolved at $\sim 1''$ resolution) radio sources are very different from those of "extended" sources. The radio emission from the core is significant for compact radio sources (Antonucci 1993; Urry & Padovani 1995) and assuming the power-law distribution of electron energies, the radio spectra of compact sources are usually flat with $\alpha_{\rm core} \leq 0.5$ (Peterson 1997). In particular for compact blazars the radio emission from the core dominates and the radio spectral index is ≈ 0.0 (Fan et al. 2010).

4 OBSERVED SPECTRAL INDEX

I derive the spectral index, α, from the measured radio emission at frequencies $\nu_{\rm TGSS} = 150\,$MHz and $\nu_{\rm NVSS} = 1.4\,$GHz for objects in the TGSS-NVSS common source catalog. For each source I compute the observed spectral index as

$$\alpha_{\rm obs} = \frac{\ln\left(\rm S_{TGSS}/S_{NVSS}\right)}{\ln\left(\nu_{\rm NVSS}/\nu_{\rm TGSS}\right)}\,, \qquad (3)$$

where $\rm S_{TGSS}$ and $\rm S_{NVSS}$ are, respectively, the flux densities measured by the TGSS and NVSS. As we have seen in Section 3.1, thermal emission is negligible and this $\alpha_{\rm obs}$ is mainly fixed by the synchrotron component.

I divide the catalog of common sources into two samples. The first low flux (LF) density sample contains sources with TGSS and NVSS flux densities below 100 mJy and 20 mJy, respectively[3]. The second high flux

[3] Note that $\rm S_{TGSS} = 100\,$mJy corresponds to $\rm S_{NVSS} \approx 20\,$mJy, assuming spectral index ≈ 0.73.

(HF) density sample includes sources above and equal to $\mathrm{S_{TGSS}} = 100\,\mathrm{mJy}$ and $\mathrm{S_{NVSS}} = 20\,\mathrm{mJy}$. These flux density cuts are imposed so that both the LF and HF samples contain roughly 50% of sources from the common source catalog. We notice from the Wilman et al. (2008) (see figure 4 therein) simulation that the LF sample is expected to consist of mostly FR I galaxies whereas the HF sample is supposed to contain an almost equal number of FR I and FR II galaxies. Furthermore, note that the TGSS ADR1 catalog is approximately complete above 100 mJy and so the HF sample represents the full radio source population (Intema et al. 2017). The LF sample is increasingly incomplete for lower flux densities. Nonetheless, the LF sample represents the sources with LF density.

The non-thermal radio emission consists mainly of synchrotron emission from jets and lobes. The spectral index from such systems is not accurately known. For jets the spectral index $\alpha_{\rm jet}$ ranges from 0.5 to 0.7 (Laing & Bridle 2013) and for lobes the non-thermal emission may be anywhere between 0.5 to 1.33 (Bell 1978; Blandford & Ostriker 1978; Kirk et al. 2000; Lemoine & Pelletier 2003; Kellermann 1966). In general we cannot isolate the radio emission from jets and lobes, however, the relative contribution from lobes dominates in large sources. For ultra-large sources and for continuous energy injection into the lobes, $\alpha_{\rm lobes}$ saturates to the value $\gamma/2$, where γ refers to electrons in the lobes.

5 RESULTS

5.1 Radio Spectral Index Dependence on Flux Density

Figures 2 and 3 show the distribution of $\alpha_{\rm obs}$ for sources with different flux density cuts and bins, respectively. Although the RMS spread is large, we see a clear trend of steepening in the spectral index with increasing flux density. The error in spectral index measurement due to flux density uncertainty is (Mahony et al. 2016b)

$$\delta\alpha = \frac{1}{\ln\frac{\nu_1}{\nu_2}}\sqrt{\left(\frac{\delta S_1}{S_1}\right)^2 + \left(\frac{\delta S_2}{S_2}\right)^2}\,, \qquad (4)$$

where $\nu_{1,2}$ and $S_{1,2}$ refer to NVSS and TGSS frequencies and flux densities respectively. The flux density accuracy in TGSS ADR1 and NVSS is $\sim$ 10% (Intema et al. 2017) and $\sim$ 5% (Condon et al. 1998), respectively. Using Equation (4), these flux density uncertainties give $\delta\alpha \sim 0.05$. However, the RMS spread observed in Figure 2 is about 0.24 which is much larger than that expected from flux density measurement uncertainty. Thus the RMS spread observed is largely the intrinsic distribution of source spectral indices. This is expected since the individual sources have very different radio emission properties, i.e. they may be FR I or FR II, and their radio flux may be largely from jets or lobes. To explore this further, I sort the sources in logarithmic bins of $\mathrm{S_{TGSS}}$ and plot the mean spectral index $\bar{\alpha}_{\rm obs}$ in each bin as a function of the flux density in Figure 4. The observed dependence is fitted by linear parametric form as indicated in the figure. This confirms the earlier hints of spectral index dependence on flux density (Gopal-Krishna & Steppe 1982; Steppe & Gopal-Krishna 1984; Windhorst et al. 1993; Prandoni et al. 2006; Ibar et al. 2009; Ishwara-Chandra et al. 2010; Randall et al. 2012). However this trend of increasing spectral index is exclusive to flux density bins of $\mathrm{S_{TGSS}}$, i.e. to low frequency bins. The trend is almost inverted if we sort the sources in logarithmic bins of $\mathrm{S_{NVSS}}$ and plot the mean spectral index (Fig. 5). This is expected and evident from Equation (3), and the fact that $\frac{d\alpha_{\rm obs}}{d\ln \mathrm{S_{TGSS}}}$ and $\frac{d\alpha_{\rm obs}}{d\ln \mathrm{S_{NVSS}}}$ are positive and negative, respectively.

The TGSS ADR1 data have high noise in the Galactic plane (Intema et al. 2017); furthermore, there are compact bright sources present in the Galactic plane (White et al. 2005) with significant thermal emission. Therefore, I mask the Galactic plane to check the robustness of the results. I find that masking the Galactic plane by 5 or 10 degrees changes $\bar{\alpha}_{\rm obs}$ in Figure 2 by a tiny value < 0.008. This is so tiny that the fit in Figure 4 remains unchanged.

A small fraction of the radio source population is known to exhibit a peaked spectrum or convex spectrum between the TGSS and NVSS frequencies (Callingham et al. 2017). These sources can be identified if the flux density is known in a large fractional bandwidth, e.g. the GaLactic and Extragalactic All-sky Murchison Widefield Array (GLEAM) catalog (Hurley-Walker et al. 2017). Ideally, I should mask all peaked-spectrum sources as these source do not follow Equation (3). However, as we only have flux densities at two frequencies, we cannot identify peaked-spectrum sources. Nevertheless, I use the Callingham et al. (2017) peaked-spectrum source catalog prepared from the GLEAM survey, which covers $\sim 60\%$ of TGSS-NVSS surveys, and identify a total of 1069 peaked and 83 convex spectrum sources in our common catalog. I mask these sources and find that the mean spectral index in Figure 2 changes by < 0.003. The remaining 40% of the TGSS-NVSS sky, not covered by GLEAM, is expected to have a similar fraction of peaked-spectrum sources, i.e. around 1000 more peaked-spectrum sources; even so we do not expect any significant change in the re-

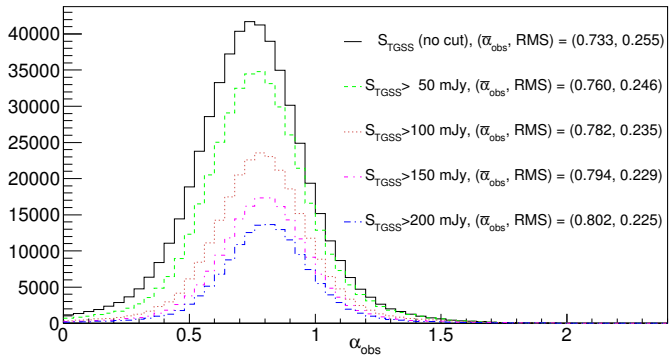

Fig. 2 The NVSS-TGSS extracted radio spectral index with various TGSS flux density cuts. The RMS is the root mean square from the $\alpha_{\rm obs}$ distribution. The TGSS ADR1 is complete above $\rm S_{TGSS} > 100\,mJy$.

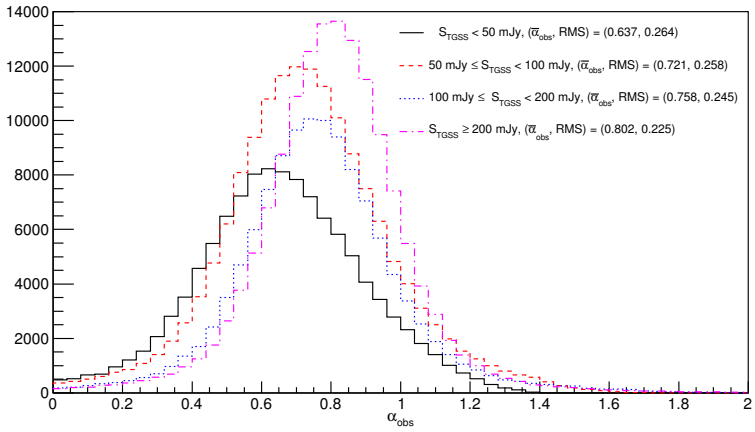

Fig. 3 The NVSS-TGSS extracted radio spectral index in various TGSS flux density bins.

sults. Furthermore, we expect a few percent of mJy radio sources to be variable on the timescale of years (Oort & Windhorst 1985; Fan et al. 2007). The unresolved compact sources, e.g. blazars, exhibit more than 4σ flux variability and constitute a small faction of the total radio population. For example, 0.1% of the unresolved sources from FIRST and NVSS are found to be variable (Ofek & Frail 2011). Similarly, Bell et al. (2019) report that $\sim 0.15\%$ of bright compact sources at low frequencies ($> 4\,$Jy at 154 MHz) show significant long-term variability. In our case, variable sources may constitute not more than a few percent of the total population and may display very steep or flat spectral index and contribute to the outliers of histograms in Figures 2 and 3; however, this is not expected to change the mean spectral index significantly.

5.2 Radio Spectral Index Dependence on Size

The size is defined as $\sqrt{ab}$ (in arcsec) where a and b are, respectively, the major and minor axes of the Gaussian fit

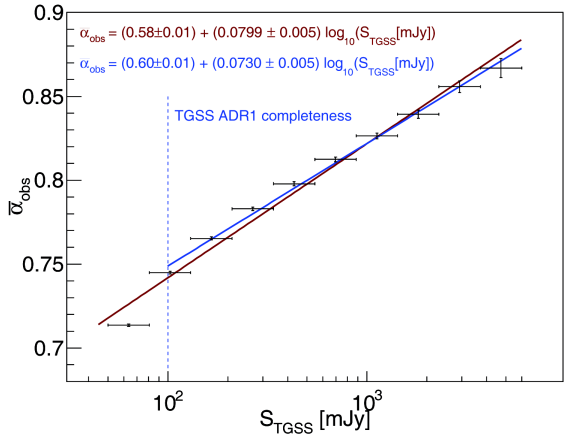

Fig. 4 The mean radio spectral index, $\bar{\alpha}_{\rm obs}$, as a function of the source TGSS flux density. The vertical error bars are the 1σ error in $\bar{\alpha}_{\rm obs}$ in each flux density bin. The horizontal error bars represent the width of each bin. The *red* and *blue lines* delineate the fits for full TGSS-NVSS common catalog and for the common catalog with TGSS ADR1 flux density completeness, respectively. Goodness of fit: $\chi^2/\rm NDF$ is 0.9649/7 (*blue*) and 5.086/8 (*red*). Corresponding p-values are 0.9954 (*blue*) and 0.7484 (*red*).

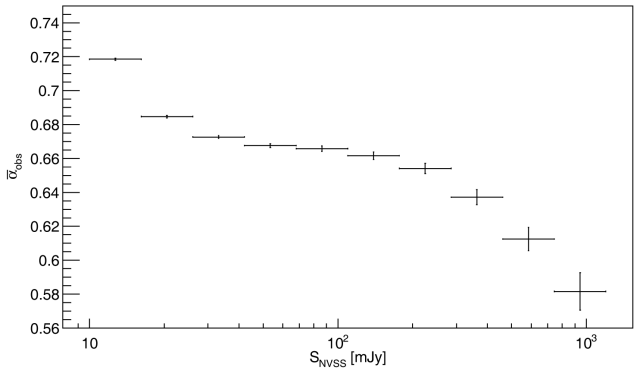

Fig. 5 The mean radio spectral index, $\bar{\alpha}_{\rm obs}$, as a function of the source NVSS flux density. The error bars have the same meaning as in Fig. 4.

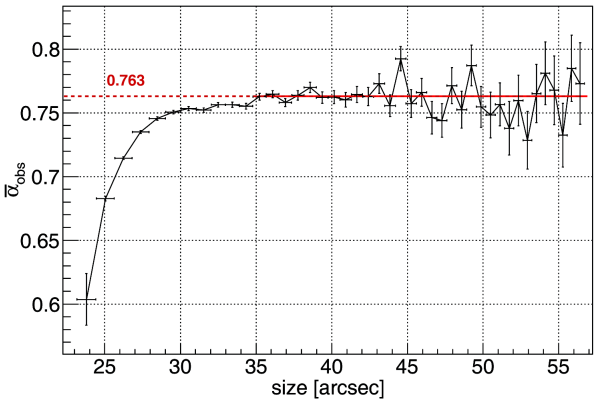

Fig. 7 The same as the previous figure but for the HF sources. The *dashed line* signifies the mean $\alpha_{\rm obs}$ from sources above $35''$. The $\alpha_{\rm obs}$ above $35''$ for HF sample is 0.763 ± 0.211.

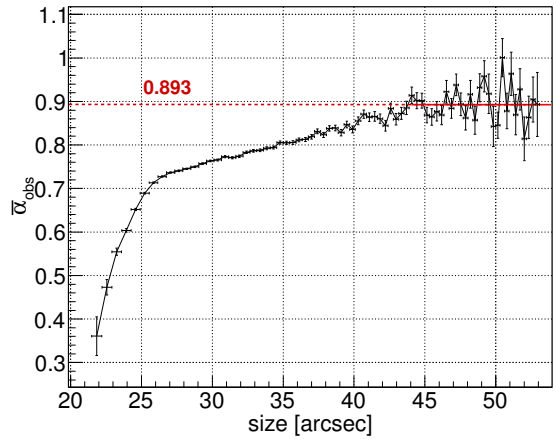

Fig. 6 The mean radio spectral index, $\bar{\alpha}_{\rm obs}$, dependence on size ($\sqrt{ab}$) for sources in the LF sample. The vertical and horizontal error bars represent the uncertainties in $\bar{\alpha}_{\rm obs}$ and the width of the bin respectively. The $\bar{\alpha}_{\rm obs}$ dependence on size saturates very clearly for sources above $44''$ (roughly 340 kpc for $z \approx 0.8$). The *dashed line* indicates the mean $\alpha_{\rm obs} = 0.893 \pm 0.223$ from sources above $44''$.

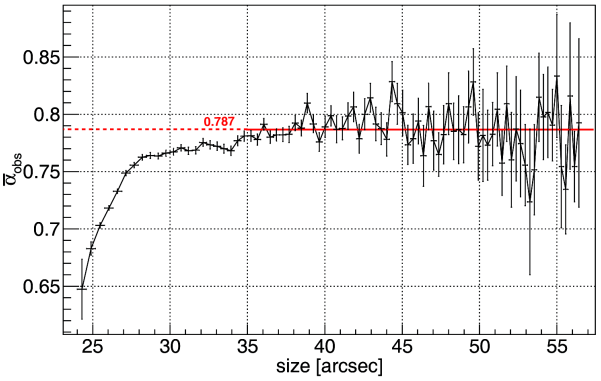

Fig. 8 The same as in Fig. 6 but for sources with TGSS flux density > 200 mJy. The *dashed line* marks the mean $\alpha_{\rm obs}$ from sources above $35''$. The $\alpha_{\rm obs}$ above $35''$ is 0.787 ± 0.205.

to the source as given in TGSS ADR1. As mentioned in Section 4, the observed spectral index consists of radio emission from jets and lobes.

Figure 6 depicts $\alpha_{\rm obs}$ as a function of size for the LF sample. The mean $\alpha_{\rm obs}$ is computed for sources lying in logarithmic bins of $\sqrt{ab}$. The spectral index increases rapidly with size until $\leq 26''$ but flattens at larger sizes, becomes nearly independent of size beyond $\sim 44''$ and saturates to the value $\alpha_{\rm obs} = 0.893 \pm 0.223$.

Figure 7 displays $\alpha_{\rm obs}$ versus $\sqrt{ab}$ for the HF sample. The spectral index increases very rapidly with source size and saturates to the limiting value $\alpha_{\rm obs} = 0.763 \pm 0.211$ at large sizes ($\gtrsim 35''$). For ultra-large sources, the emission is lobe dominated and therefore $\alpha_{\rm obs}$ represents the spectral index from lobes. Finally, I plot the $\alpha_{\rm obs}$ size dependence for sources above and equal to $S_{\rm TGSS} = 200$ mJy and $S_{\rm NVSS} = 40$ mJy in Figure 8. The spectral index saturates to the limiting value $\alpha_{\rm obs} = 0.763 \pm 0.211$ above sizes $\gtrsim 35''$. For these HF density limits, we can be very certain about TGSS completeness.

6 SUMMARY AND DISCUSSION

I have computed the radio spectral index from a catalog of about half a million common sources in NVSS and TGSS. The flux density accuracy in the common catalog is better than 10% which is sufficient for the studies performed in this paper. I check the robustness of the results with Galactic plane cuts and find no significant change. I also mask the known peaked-spectrum sources identified from the GLEAM survey covering $\sim 60\%$ of the common catalog and find no significant change in the results. We have a relatively small number of sources close to survey resolution, i.e. with size $< 25''$ ($\sim 5\%$ and 1% of LF and

HF sample, respectively) and some fraction of these small size sources may belong to the Compact Steep Spectrum (CSS) and Gigahertz Peaked Spectrum (GPS) population (O'Dea 1998; Snellen et al. 2000). In particular, we observe the very flat spectral index (< 0.5) for very compact sources in the LF sample. This is likely to be the result of significant CSS or GPS population (Mahony et al. 2016a,b). Also, with extreme sizes (small or very large) the orientation is less likely to be randomly oriented. This altogether may introduce some bias in the observed spectral index and the results may be relatively less reliable for sources with extreme sizes. The saturated spectral index for both LF and HF samples is robust and independent of these possible systematics and biases though.

I divide the catalog into two flux density limited samples, LF and HF. The large number of sources enables us to study the spectral index in differential size bins. The spatially integrated radio spectral index, relevant to this work, consists of radio emission from lobes and jets. I explore the source size dependence of observed spectral index and draw the following conclusions:

- I confirm the steepening of the radio spectral index in the low frequency bins with increasing flux density (Gopal-Krishna & Steppe 1982; Steppe & Gopal-Krishna 1984; Windhorst et al. 1993; Prandoni et al. 2006; Ibar et al. 2009; Ishwara-Chandra et al. 2010; Randall et al. 2012). This trend is inverted if we sort the sources in high frequency flux density bins.
- The spectral index becomes nearly independent of source size above $\sim 44''$ for LF sample and above $\sim 35''$ for HF sample. The saturated spectral index for both LF and HF samples is in between $0.75 - 0.90$, consistent with previous studies (Intema et al. 2011; Williams et al. 2013, 2016; Hardcastle et al. 2016; Mahony et al. 2016b). Both samples are hosts of AGNs, although the LF sample is presumably dominated by FR I galaxies (Wilman et al. 2008). Assuming that the sources lie at redshifts $z \approx 0.8$, $44''$ size corresponds to ~ 340 kpc (assuming standard ΛCDM cosmology and using cosmological parameters from Planck Collaboration et al. (2016)). For very compact sources in the LF sample, the observed spectral index is flatter, ~ 0.4, which hints at a significant thermal component from the nucleus in total radio emission for these compact sources. Alternatively, a significant fraction of these compact sources may belong to the CSS and GPS populations. The CSS and GPS sources may manifest a very flat 150 MHz – 1.4 GHz spectral index (Mahony et al. 2016a,b). The LF sample is increasingly incomplete for LF densities; even so the results qualitatively represent the low flux density radio sources.
- HF sample exhibits a very strong dependence of the spectral index on size below $\sim 35''$. This is likely due to an increasing fraction of jets and nuclear radio emission in comparison to emission from lobes. The sources with larger sizes reach a saturated spectral index $\alpha_{\rm obs} = 0.763 \pm 0.211$. The radio emission from these large sources is lobe dominated and so the observed spectral index can be seen as characteristic of radio emission from lobes.
- The saturated spectral index for the LF sample is steeper than that for the HF sample. The LF sample is predominantly FR I (Wilman et al. 2008) and the lobes in these galaxies exhibit the steepest spectra (Kembhavi & Narlikar 1999). The electrons in the lobes are most retarded and aged. In comparison with the HF sample, we see a relatively slow rise of spectral index with size for the LF sample. However, I remind the reader that the LF sample is increasingly incomplete for LF densities and this slow rise of spectral index may be the result of incompleteness. The sharp saturation of spectral index for the HF sample, which contains an almost equal number of FR I and FR II galaxies (Wilman et al. 2008), indicates very clear domination of radio emission from lobes for these bright galaxies.

Acknowledgements I thank Adi Nusser and Ari Laor for discussion and their extensive and thoughtful comments on this work, and the anonymous referee for useful comments that helped to improve the paper. I especially thank Huib T. Intema for help with the TGSS ADR1 catalog. This work is supported by the NAOC Youth Talent Fund (110000JJ01). I have used CERN ROOT 5.34/21 (Brun et al. 2001) for generating plots.

References

Antonucci, R. 1993, ARA&A, 31, 473
Bell, A. R. 1978, MNRAS, 182, 147
Bell, M. E., Murphy, T., Hancock, P. J., et al. 2019, MNRAS, 482, 2484
Biermann, P. 1976, A&A, 53, 295
Blandford, R. D., & Königl, A. 1979, ApJ, 232, 34
Blandford, R. D., & Ostriker, J. P. 1978, ApJ, 221, L29
Bridle, A. H., & Perley, R. A. 1984, ARA&A, 22, 319

Brun, R., Rademakers, F., et al. 2001, (ROOT web page, *http://root.cern.ch/*)
Callingham, J. R., Ekers, R. D., Gaensler, B. M., et al. 2017, ApJ, 836, 174
Condon, J. J. 1992, ARA&A, 30, 575
Condon, J. J., Cotton, W. D., Greisen, E. W., et al. 1998, AJ, 115, 1693
Condon, J. J., & Yin, Q. F. 1990, ApJ, 357, 97
De Young, D. S. 1976, ARA&A, 14, 447
Fan, J.-H., Yang, J.-H., Tao, J., Huang, Y., & Liu, Y. 2010, PASJ, 62, 211
Fan, J. H., Liu, Y., Yuan, Y. H., et al. 2007, A&A, 462, 547
Fanaroff, B. L., & Riley, J. M. 1974, MNRAS, 167, 31P
Gopal-Krishna, & Steppe, H. 1982, A&A, 113, 150
Hardcastle, M. J., Gürkan, G., van Weeren, R. J., et al. 2016, MNRAS, 462, 1910
Harwood, J. J., Hardcastle, M. J., & Croston, J. H. 2015, MNRAS, 454, 3403
Harwood, J. J., Hardcastle, M. J., Croston, J. H., & Goodger, J. L. 2013, MNRAS, 435, 3353
Harwood, J. J., Croston, J. H., Intema, H. T., et al. 2016, MNRAS, 458, 4443
Harwood, J. J., Hardcastle, M. J., Morganti, R., et al. 2017, MNRAS, 469, 639
Hurley-Walker, N., Callingham, J. R., Hancock, P. J., et al. 2017, MNRAS, 464, 1146
Ibar, E., Ivison, R. J., Biggs, A. D., et al. 2009, MNRAS, 397, 281
Intema, H. T., Jagannathan, P., Mooley, K. P., & Frail, D. A. 2017, A&A, 598, A78
Intema, H. T., van Weeren, R. J., Röttgering, H. J. A., & Lal, D. V. 2011, A&A, 535, A38
Ishwara-Chandra, C. H., Sirothia, S. K., Wadadekar, Y., Pal, S., & Windhorst, R. 2010, MNRAS, 405, 436
Kellermann, K. I. 1966, ApJ, 146, 621
Kembhavi, A. K., & Narlikar, J. V. 1999, Quasars and Active Qalactic Nuclei: an Introduction (Cambridge: Cambridge Univ. Press)
Kirk, J. G., Guthmann, A. W., Gallant, Y. A., & Achterberg, A. 2000, ApJ, 542, 235
Laing, R. A., & Bridle, A. H. 2013, MNRAS, 432, 1114
Laing, R. A., & Bridle, A. H. 2014, MNRAS, 437, 3405
Lal, D. V. 2013, GMRT Observer's Manual, Available at *http://gmrt.ncra.tifr.res.in/gmrt_hpage/Users/doc/manual/Manual_2013/manual_20Sep2013.pdf* (November 18, 2013)
Lemoine, M., & Pelletier, G. 2003, ApJ, 589, L73
Mahony, E. K., Morganti, R., Prandoni, I., van Bemmel, I., & LOFAR Surveys Key Science Project, 2016a, Astronomische Nachrichten, 337, 135
Mahony, E. K., Morganti, R., Prandoni, I., et al. 2016b, MNRAS, 463, 2997
Nusser, A., & Tiwari, P. 2015, ApJ, 812, 85
O'Dea, C. P. 1998, PASP, 110, 493
Ofek, E. O., & Frail, D. A. 2011, ApJ, 737, 45
Oort, M. J. A., & Windhorst, R. A. 1985, A&A, 145, 405
Peterson, B. M. 1997, An Introduction to Active Galactic Nuclei (Cambridge: Cambridge Univ. Press)
Planck Collaboration, Ade, P. A. R., Aghanim, N., et al. 2016, A&A, 594, A13
Prandoni, I., Parma, P., Wieringa, M. H., et al. 2006, A&A, 457, 517
Randall, K. E., Hopkins, A. M., Norris, R. P., et al. 2012, MNRAS, 421, 1644
Snellen, I. A. G., Schilizzi, R. T., Miley, G. K., et al. 2000, MNRAS, 319, 445
Steppe, H., & Gopal-Krishna. 1984, A&A, 135, 39
Swarup, G. 1991, in Astronomical Society of the Pacific Conference Series, 19, IAU Colloq. 131: Radio Interferometry. Theory, Techniques, and Applications, eds. T. J. Cornwell, & R. A. Perley, 376
Tiwari, P., & Nusser, A. 2016, Journal of Cosmology and Astro-Particle Physics, 2016, 062
Urry, C. M., & Padovani, P. 1995, PASP, 107, 803
White, R. L., Becker, R. H., & Helfand, D. J. 2005, AJ, 130, 586
Williams, W. L., Intema, H. T., & Röttgering, H. J. A. 2013, A&A, 549, A55
Williams, W. L., van Weeren, R. J., Röttgering, H. J. A., et al. 2016, MNRAS, 460, 2385
Wilman, R. J., Miller, L., Jarvis, M. J., et al. 2008, MNRAS, 388, 1335
Windhorst, R. A., Fomalont, E. B., Partridge, R. B., & Lowenthal, J. D. 1993, ApJ, 405, 498